A modeling study of water and salt exchange for a micro-tidal, stratified northern Gulf of Mexico estuary

Article *in* Journal of Marine Systems · August 2012

DOI: 10.1016/j.jmarsys.2012.02.008

CITATIONS
65

READS
350

2 authors, including:

Kyeong Park
Texas A&M University - Galveston
76 PUBLICATIONS **1,343** CITATIONS

SEE PROFILE

Journal of Marine Systems 96–97 (2012) 103–115

Contents lists available at SciVerse ScienceDirect

Journal of Marine Systems

journal homepage: www.elsevier.com/locate/jmarsys

A modeling study of water and salt exchange for a micro-tidal, stratified northern Gulf of Mexico estuary

Choong-Ki Kim [1], Kyeong Park *

Department of Marine Sciences, University of South Alabama, Dauphin Island Sea Lab, 101 Bienville Blvd., Dauphin Island, AL 36528, USA

ARTICLE INFO

Article history:
Received 9 June 2011
Received in revised form 4 November 2011
Accepted 19 February 2012
Available online 4 March 2012

Keywords:
Salt transport
Stratification
River discharge
Wind
Hydrodynamic modeling
Mobile Bay, USA
Northern Gulf of Mexico
88°30.18′–87°41.35′W, 29°50.70′–31°05.03′N

ABSTRACT

A three-dimensional hydrodynamic model is applied to the Mobile Bay system to study water and salt exchange with the northern Gulf of Mexico via Main Pass (MP) and eastern Mississippi Sound via Pass-aux-Herons (PaH). On average, more water leaves the Bay through MP than through PaH, and the Bay gains salt through MP and loses about the same amount through PaH. However, the volume discharge rate Q_f and salt transport rate F_S vary greatly in response to wind and river discharge with the range of variation 1–2 orders of magnitude larger than the corresponding mean. Stratification plays a key role for salt transport through MP. During periods of large river discharge, the landward shear dispersive transport F_E peaking during equatorial tides and the landward tidal oscillatory transport F_T peaking during tropic tides, respectively, balance the seaward advective transport $Q_f S_0$. During periods of relatively weak stratification, F_S at MP is almost entirely determined by $Q_f S_0$ and its variability is well correlated with north–south (along-estuary) wind, associated with the barotropic (water level) adjustment. At the shallow, weakly stratified PaH, F_S is almost identical to $Q_f S_0$, and Q_f is well correlated with east–west wind, with the correlation becoming stronger during the dry period.

1. Introduction

Subtidal exchange between an estuary and the adjacent coastal shelf determines the long-term transport of water and mass to and from the estuary. The exchange affects many important processes, including flushing capacity of an estuary, residence time of land-derived pollutants, retention of autochthonous materials, and ingress of planktonic larvae (Hare et al., 2005; Lowery, 1988; MacDonald, 2006; Sheldon and Alber, 2002; Simons et al., 2006). Recently, during the Deepwater Horizon oil spill of 2010, this exchange was a critical topic of concern as oil and oil-derived substances were transported into the estuaries and bays along the northern Gulf of Mexico.

The characteristics of estuary–shelf, or estuary–subestuary, exchange have been studied in many estuaries for various forcing functions such as wind, gravitational circulation, tidal action, freshwater discharge, and cross-sectional bathymetry of the estuarine mouth (Goodrich, 1988; Valle-Levinson and Lwiza, 1995; Valle-Levinson et al., 2001, 2009; Wiseman et al., 1988; Wong and Moses-Hall, 1998). These studies show that it is the lateral and vertical structure of flow and mass distribution across a cross-section that determines the exchange of water and mass. Consequently, estimation of the exchange dynamics at both average and event time scales requires long-term data with high spatial and temporal resolution.

Many estuaries along the northern Gulf of Mexico share several common attributes, including: shallow and wide basins, deep and narrow ship channels, diurnal tides with a micro-tidal range, relatively large river discharge, and water exchange with the Gulf of Mexico via relatively narrow passes (Schroeder and Wiseman, 1999). Mobile Bay, Alabama is one such system, connected to the northern Gulf via Main Pass (MP) and to eastern Mississippi Sound via Pass-aux-Herons (PaH) (Fig. 1). Two previous studies have estimated mean water exchange through the two passes. Austin (1954) estimated that MP may handle approximately 67–75% of the total volume of water flushed into or out of Mobile Bay, and PaH the remaining 25–33%. Schroeder (1978) suggested that MP may be responsible for approximately 85% of the water exchange and PaH the remaining 15%. In terms of driving shelf–estuarine water exchange through MP, subsequent studies based on water level data (Schroeder and Wiseman, 1986) and one-month current data (Wiseman et al., 1988) have shown that the along-shore and cross-shore winds become important at periods of 2–20 d and river discharge at seasonal scales. No observational or modeling study has yet been conducted to address the dynamics of salt (mass) exchange for Mobile Bay.

The importance of shelf–estuary exchange has been noted for the northern Gulf of Mexico estuaries, in the context of larval transport, nutrient budget, sediment plumes, organic matter, etc. (Lohrenz et al., 1997; Morgan et al., 1996; Mortazavi et al., 2000; Rabalais et al., 1995; Spitzer et al., 2003; Stumpf et al., 1993). However,

* Corresponding author. Tel.: +1 251 861 2141x7563; fax: +1 251 861 7540.
E-mail address: kpark@disl.org (K. Park).
[1] Present address: Department of Biology, Stanford University, 371 Serra Mall, Stanford, CA 94305, USA.

0924-7963/$ – see front matter © 2012 Elsevier B.V. All rights reserved.
doi:10.1016/j.jmarsys.2012.02.008

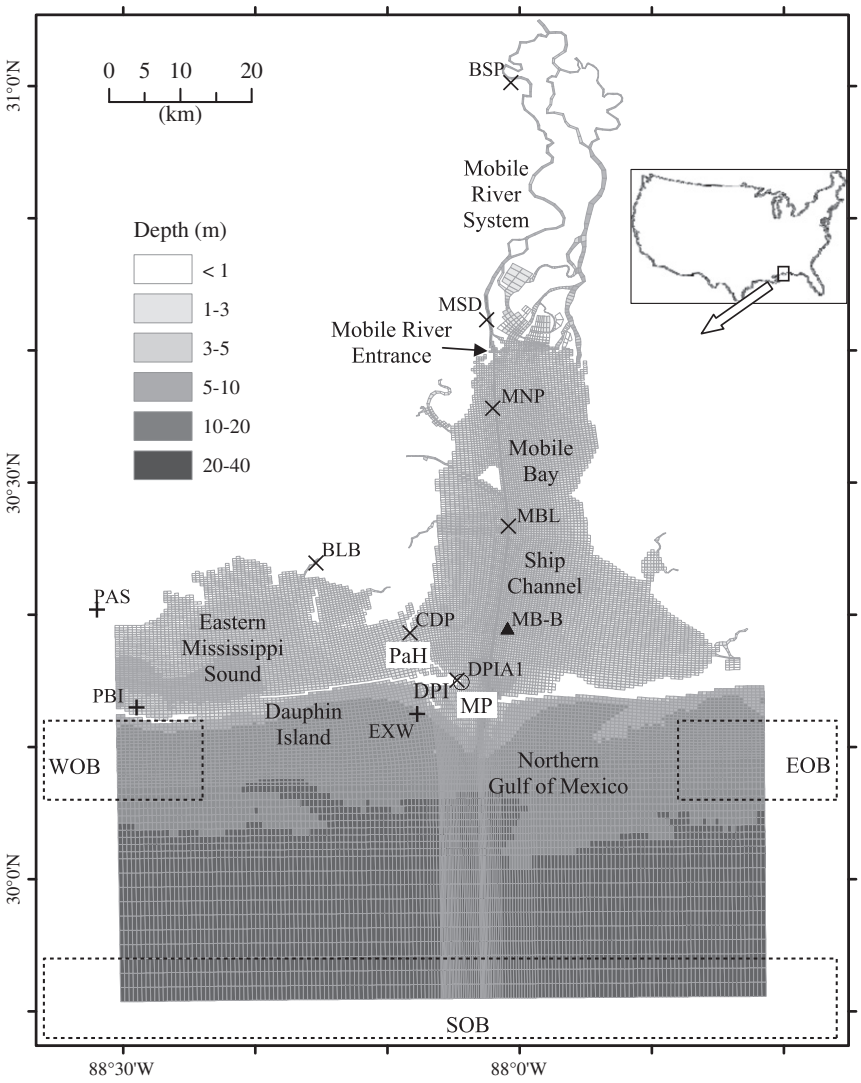

Fig. 1. A grid for Mobile Bay connected to the northern Gulf of Mexico through Main Pass (MP) and to eastern Mississippi Sound through Pass-aux-Herons (PaH), showing a meteorological station for wind, DPIA1 (○), tide stations used for the water level open boundary condition (+), seven tide stations for surface elevation data (×), and a station for velocity and salinity data (▲). Dotted boxes for SOB, WOB, and EOB indicate the areas where the salinity open boundary conditions are estimated based on the NODC data.

some questions regarding the dynamics of water and salt exchange itself remain unanswered, primarily because of lack of data with the necessary spatial/temporal resolution and temporal duration. The collection of long-term data is unfeasible at MP because mooring instruments is prohibited in the federally managed ship channel, which makes the application of a numerical model a reasonable alternative.

Here, we present the application of a three-dimensional hydrodynamic model to study the dynamics of water and salt exchange through MP and PaH. We first describe the model and its set-up (Section 2), followed by the model validation with field data (Section 3). We then use the model results to study the characteristics of water and salt exchange (Section 4). The goals of this study are to examine the primary mechanisms that drive water and salt transport through MP and PaH, and their variability under different forcing conditions.

2. Methodology

2.1. Model description

We employ the hydrodynamic model in the Three-dimensional Hydrodynamic-Eutrophication Model (HEM3D), also referred to as the Environmental Fluid Dynamics Code (EFDC). The model is based on turbulence-averaged governing equations, including continuity, momentum, salt-balance, and heat-balance equations with hydrostatic and Boussinesq approximations (Hamrick, 1992). The spatial density gradient is almost entirely determined by the salinity gradient in the study area (Park et al., 2007), thus the present model application does not solve the heat-balance equation and instead calculates density solely as a function of salinity. For turbulence closure, the model employs the second moment turbulence model developed by Mellor and Yamada (1982) and modified by Galperin et al. (1988). The model uses orthogonal curvilinear or Cartesian horizontal coordinates and a stretched sigma vertical coordinate. One of the unique features in the numerical solution of the model is an internal–external mode splitting for the momentum equation. The model solves both modes using the same time step by solving the external mode semi-implicitly with respect to the barotropic pressure gradient terms in the depth-averaged momentum equations, which allows large time steps and facilitates the wetting-and-drying scheme (Ji et al., 2001). A more detailed description of the model, including the governing equations, numerical solution method, and handling of open boundary conditions, can be found in Hamrick (1992, 1996).

2.2. Modeling domain and grid system

Mobile Bay is a broad, shallow (average depth of 3 m) estuary with a narrow (120 m) and deep (12–14 m) ship channel (Fig. 1). The hydrodynamic conditions in Mobile Bay and eastern Mississippi Sound are influenced by fluctuations in coastal sea level that includes tides, river discharge, and wind, with their relative impacts varying temporally and spatially (Noble et al., 1996; Schroeder and Lysinger, 1979; Wiseman et al., 1988). The tide is predominantly diurnal with a tropic–equatorial cycle where the tidal range varies from <0.1 m during equatorial tides to 0.8 m during tropic tides. The tropic–equatorial cycle (period of 13.66 d) is a modulation in tidal range in diurnal tidal systems due to the phasing in-and-out of the principal diurnal constituents of K_1 and O_1, whereas the spring–neap cycle (period of 14.76 d) is in semidiurnal systems due to the phasing in-and-out of the M_2 and S_2 constituents (Boon, 2004). Mobile Bay receives 95% of its freshwater input from the Mobile River system, the fourth largest river discharge in the U.S. (Schroeder, 1978). Long-term (1976–2006) mean river discharge is 1762 $m^3 s^{-1}$ with relatively high discharge occurring in December–May and low discharge in June–November. Variations in river discharge affect the salinity regime and gravitational circulation that exists in the deeper portions of Mobile Bay including the ship channel (Schroeder and Lysinger, 1979; Wiseman et al., 1988). Wind is an important driving and modifying forcing mechanism for circulation and vertical mixing in shallow Mobile Bay, and shows distinct seasonal variation. A southerly wind is dominant in spring and summer, and a stronger northerly wind is dominant in fall and winter (Noble et al., 1996; Schroeder and Wiseman, 1986).

The hydrodynamic model has been applied to the study area (88°30.18′–87°41.35′W, 29°50.70′–31°05.03′N) that includes Mobile Bay, the Mobile River system, eastern Mississippi Sound, and the northern Gulf of Mexico (Fig. 1). The modeling domain is 80 km × 136 km in the east–west and north–south directions, respectively. The seaward open boundary is extended southward to about 45 km south of Dauphin Island and the upriver boundary is at Mount Vernon. A grid system is generated using shoreline data from NOAA's Coastal Services Center and bathymetry data from the northern Gulf of Mexico Littoral Initiative and the Mobile District of the U.S. Army Corps of Engineers (USACE). An orthogonal curvilinear grid is used to resolve the complex shoreline and bottom topography in the Mobile River system and the inner portion of the Bay. The grid system has 21,705 surface water cells and five vertical sigma layers, with the grid size varying from 58 to 2000 m. The finest grid cells are small enough to resolve the narrow ship channel, represented by three continuous grid indices to ensure a more accurate simulation of mass transport along the channel.

2.3. Initial and boundary conditions

Application of the model requires specification of input parameters for initial conditions (surface elevation, velocity, and salinity), upriver and surface boundary conditions (river discharge and wind), and open boundary conditions (surface elevation and salinity).

With arbitrary (zero) initial conditions for surface elevation and velocity (i.e., cold start), the model becomes stabilized within a few tidal cycles. To estimate the initial conditions for salinity, an ideal model run is conducted forced with harmonic tides with the two most important diurnal constituents ($K_1 + O_1$), 31-year (1976–2006) median river discharge, and 20-year (1987–2006) median wind speed with a random wind direction. The tidal average salinity field calculated after the ideal model run reaches steady state is used for the initial condition, which is specified after five days of initial warming up from the cold start.

Daily freshwater discharge data from two gauging stations, Claiborne Lock and Dam in Alabama River and Coffeeville Lock and Dam in Tombigbee River, are obtained from the U.S. Geological Survey. Their sum is used as the total freshwater discharge into Mobile Bay, following Park et al. (2007). Hourly wind data at the Dauphin Island Station (DPIA1 in Fig. 1) are obtained from NOAA's National Data Buoy Center and are used for the surface boundary conditions.

We estimate the open boundary condition for water level using the USACE's time series data at Exxon Well (EXW), Petit Bois Island (PBI), and Pascagoula (PAS) (Fig. 1). The data at EXW are used for all open boundary cells in the northern Gulf of Mexico. The western open boundary condition for the cells within eastern Mississippi Sound is estimated using linear interpolation between the data at PBI and PAS. Because the model results agree very well with the observed surface elevation throughout the modeling domain, no correction is made for the water level open boundary condition. When the USACE's data are unavailable, surface elevation data from NOAA's tide station at Dauphin Island (DPI in Fig. 1) are used for all open boundary cells after being adjusted using correction factors for amplitude and phase. The correction factors are estimated from differences in amplitude and phase between the model results and the DPI data. The model simulations forced with the USACE's data and the adjusted NOAA data show very little difference (mean difference <1 cm).

We estimate the open boundary condition for salinity using the 1970–2000 data from National Oceanographic Data Center (NODC). Table 1 lists the mean salinities calculated for the surface and bottom layers of SOB, WOB, and EOB (defined in Fig. 1). Vertical salinity profiles for five sigma layers are constructed using the mean values and assuming homogeneity between the surface and the 2nd layer and between the 4th and the bottom layer, with the salinity in the 3rd layer linearly interpolated. The vertical salinity profile in SOB is specified for the southern open boundary cells. The linearly interpolated salinity profile between SOB and WOB is specified for the western open boundary cells in the northern Gulf of Mexico, and the linearly extrapolated salinity profile is specified for the remaining western open boundary cells within eastern Mississippi Sound. The linearly interpolated salinity profile between SOB and EOB is specified for the eastern open boundary cells. The salinity open boundary condition remains constant in time. The present model employs the specified salinity values for inflowing water and outflowing values are calculated using upwinded values immediately inside the open boundary (Hamrick, 1996).

3. Model-data comparison

The data used for model validation are summarized in Table 2, with the station locations shown in Fig. 1. A barotropic model run is conducted for 75 d (September 16 and November 29, 2000), and the model results are compared with hourly surface elevation data at the seven tide stations including DPI, Cedar Point (CDP), Bayou La Batre (BLB), Middle Bay Light (MBL), McNally Point (MNP), Mobile State Dock (MSD), and Barry Steam Plant (BSP). A baroclinic model run is conducted for 270 d (April 6 and December 31, 1991), and the model results are compared with hourly current velocity and salinity data at station MB-B. The model results are compared with the data for both total and subtidal (48-h low-pass filtered) components. As quantitative assessments for the model-data comparison,

Table 1
Mean and standard deviation of salinity at the surface and bottom layers of three open boundary areas using the NODC data in 1970–2000.

Open boundary[a]	Surface[b]		Bottom[b]	
	Mean ± SD[c]	N[c]	Mean ± SD	N
SOB	33.4 ± 1.9	445	35.7 ± 0.6	110
WOB	28.9 ± 3.3	35	33.5 ± 2.0	21
EOB	31.1 ± 0.8	8	32.9 ± 0.4	5

[a] See Fig. 1 for locations.
[b] Surface and bottom layers of five sigma layers.
[c] Mean, standard deviation (SD), and the number (N) of observations.

Table 2
Data for model validation.

Variable	Station[a]	Time period	Depth[b]	Source
Surface elevation	7 tide stations	16/09–29/11 in 2000	–	USACE[c]
Current velocity	MB-B	17/05–01/08 in 1991	Surface Bottom	WRDB[d]
Salinity	MB-B	07/08–07/10 in 1991	Surface Bottom	WRDB[d]

[a] See Fig. 1 for station locations.
[b] Surface (1.0 m) and bottom (3.4 m).
[c] Mobile District of the U.S. Army Corps of Engineers.
[d] Mobile Bay Water Resources Database, EPA Region IV.

the mean error (*ME*), mean absolute error (*MAE*), and predictive skill (*Skill*) are given in Table 3, which are defined as (Willmott, 1982):

$$ME = \frac{\sum (M_n - O_n)}{N} \tag{1a}$$

$$MAE = \frac{\sum |M_n - O_n|}{N} \tag{1b}$$

$$Skill = 1 - \frac{\sum (M_n - O_n)^2}{\sum \left(|M_n - \overline{O}| + |O_n - \overline{O}| \right)^2} \tag{1c}$$

where M_n and O_n are the nth model result and observation, respectively, with $\overline{O}$ indicating a time mean data, and N is the number of observations. *ME* indicates over-prediction (positive *ME*) or under-prediction (negative *ME*) on average. The magnitude of *MAE* indicates the average deviation between model and data. *Skill* provides an index of model-data agreement, with a skill of one indicating perfect agreement and a skill of zero indicating complete disagreement.

3.1. Surface elevation

The model application with a bottom roughness height of 0.2 cm gives an excellent reproduction of the observed surface elevation, with an overall *ME* of −1 cm, *MAE* of 2–4 cm, and model skill of 0.99 (Table 3). The model results agree very well with both the total and subtidal components at the seven stations throughout the modeling domain. The model reproduces tidal variations well, including tropic-equatorial modulation in tidal range and propagation of tidal waves (Fig. 2). The model also successfully reproduces surface set-down and set-up in response to river discharge and wind (Fig. 3). Both data and model show that increased river discharge toward the end of model run affects surface elevation, resulting in an increase in surface slope between BSP and DPI, particularly beyond day 328. River influence is mostly confined to the northern portion of the Bay resulting in an increase in along-Bay surface slope, which Schroeder and Wiseman (1986) attributed to widening of the Bay to the south and flushing out of freshwater through MP and PaH.

Previous studies noted the importance of wind for modifying surface slope and thus the subtidal response of Mobile Bay. North–south wind directly alters along-Bay surface slope and thus produces barotropic circulation within Mobile Bay at periods of 2–4 d (Schroeder and Wiseman, 1986), and about 40% of the variability in along-Bay surface slope is associated with north–south wind stress (Noble et al., 1996). Both data and model show that relatively strong north wind causes surface set-down on days 268–273, 279–286, and 318–328, and relatively strong south wind causes surface set-up on days 309–314 (Fig. 3). The surface set-up and set-down occurs at all seven stations, with the disturbance propagating in the direction of wind. The degree of surface disturbance increases upstream regardless of wind direction, probably due to the geometric convergence, resulting in the modification of along-Bay surface slope. A good reproduction of the Bay-wide variation in surface elevation and the resulting surface slope indicates that the present model application provides a good simulation of the tidal and subtidal response of Mobile Bay to variations in forcing functions.

3.2. Current velocity

The model reproduces variations in current velocity well (Fig. 4c). For the total velocity components, *ME* is small ranging from −2 to 1 cm s^{-1} and *MAE* ranges from 6 to 8 cm s^{-1} (Table 3). Both data and model show that the *u* and *v* velocity components are comparable near the surface. The model has high predictive skills of 0.91–0.92 in simulating the surface *u* and *v* velocities although the model slightly under-predicts surface *u* velocity while slightly over-predicts surface *v* velocity. Both data and model show that north–south direction becomes the principal axis near the bottom, and the model has a skill of 0.91 for the principal axis component (bottom *v*) but a somewhat lower skill of 0.79 for bottom *u* velocity. Highly sheared current, with velocity shear as strong as either surface or bottom velocity, has been observed in Mobile Bay (Noble et al., 1996; Park et al., 2007). The model reproduces the observed strong velocity shear well (Fig. 4c).

Table 3
Error estimates for model-data comparison.

Variables		Station[a]	Total component				Subtidal component			
			ME[b]	*MAE*[b]	*Skill*[b]	*N*	*ME*	*MAE*	*Skill*	*N*
Surface elevation (cm)		BSP	−2	5	0.98	1668	−1	2	0.99	1572
		MSD	−2	5	0.99	1680	−2	2	0.99	1632
		MNP	1	5	0.98	1680	1	4	0.99	1632
		MBL	−1	4	0.99	1658	−1	2	0.99	1579
		BLB	−1	2	0.99	1680	−1	2	0.99	1632
		CDP	−1	3	0.99	1680	−1	2	0.98	1632
		DPI	−2	2	0.99	1680	−2	2	0.99	1632
		Overall	−1	4	0.99	11,726	−1	2	0.99	11,311
Current velocity (cm s^{-1})	*u* (surf)	MB-B	−1	6	0.91	1736	−1	3	0.85	1640
	v (surf)		−1	8	0.92	1736	−1	3	0.78	1640
	u (bot)		1	6	0.79	1293	1	2	0.65	1149
	v (bot)		−2	7	0.91	1293	−2	3	0.76	1149
Salinity (psu)	(surf)	MB-B[d]	1	2	0.82	1143	1	2	0.68	1095
	(bot)		1	2	0.80	1143	1	2	0.77	1095
	(diff[c])		−1	2	0.81	1143	−1	1	0.82	1095

[a] See Fig. 1 for station locations.
[b] *ME* (mean error), *MAE* (mean absolute error), and *Skill* (predictive skill) are defined in Eq. (1).
[c] Bottom-surface salinity difference.
[d] Errors estimated without including the time period of 225–238 d (see Section 3.3).

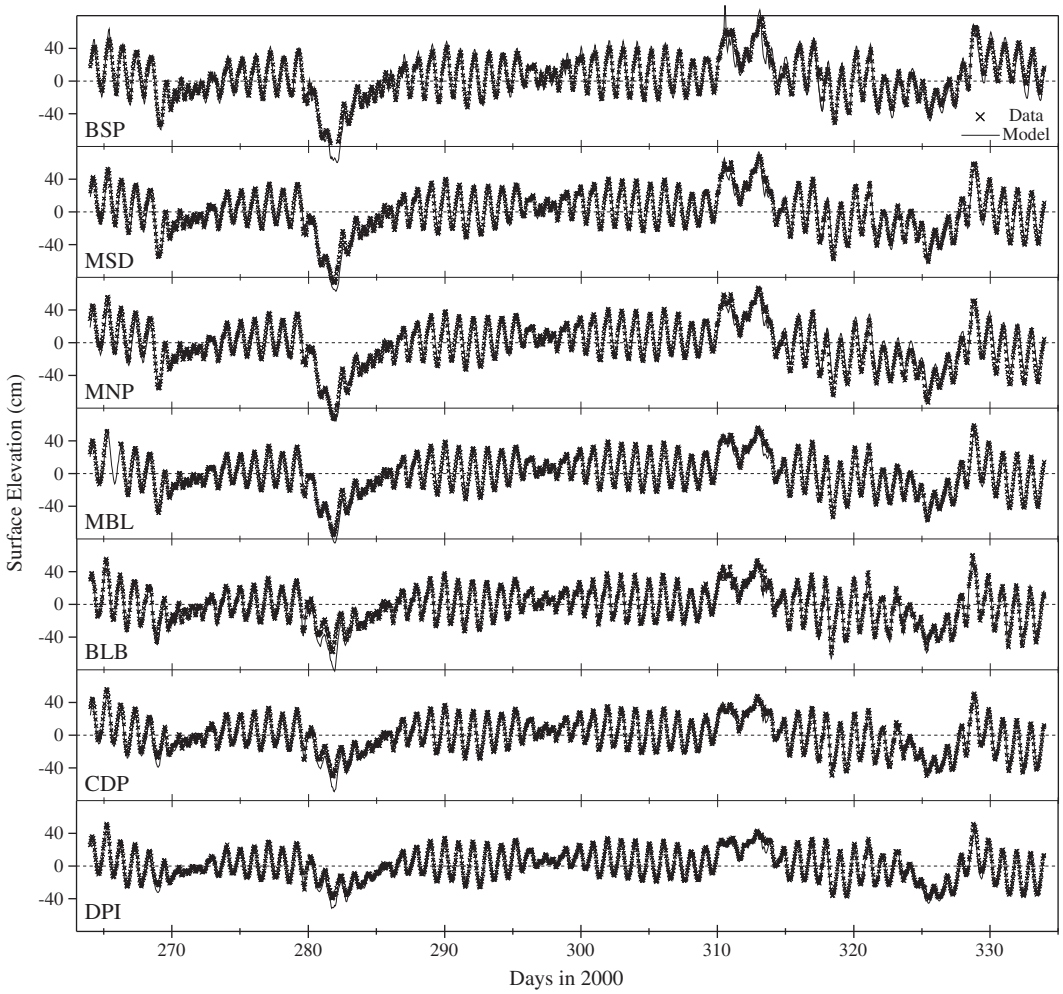

Fig. 2. Model-data comparison for surface elevation at seven tide stations.

The model also reproduces variations in the subtidal velocity well (Fig. 4d), with *ME* ranging from −2 to 1 cm s^{-1} and *MAE* ranging from 2 to 3 cm s^{-1} (Table 3). The modeled subtidal current flows in the same direction as the observed subtidal current most of the time, with the predictive skills of 0.76–0.85 for surface and bottom *v* (principal axis) velocities. The model skill is somewhat low at 0.65 for bottom *u* velocity.

Noble et al. (1996) noted two response patterns of current velocity to river discharge in lower Mobile Bay. A weak to moderate river discharge drives downstream current in the surface layer but not in the bottom layer, thus increasing velocity shear. A large river discharge >3000 $m^3 s^{-1}$, however, produces downstream current in the bottom layer such that both surface and bottom currents flow downstream. Both data and model show these two response patterns (Fig. 4d). When river discharge is <3000 $m^3 s^{-1}$ (days 180–215), downstream flow (i.e., negative *v*) is more apparent in the surface layer than in the bottom layer. When river discharge is >3000 $m^3 s^{-1}$ (days 135–159), downstream flow is apparent in both surface and bottom layers. Noble et al. (1996) also noted sheared current velocity driven by wind for stratified water column. During conditions when the bottom-surface salinity difference >5 psu over a vertical distance of 2.2 m, the wind-induced current pattern is highly sheared with oppositely directed surface and bottom currents. Both data and model show that east wind stress>0.1 Pa on days 139–143 and 157–160 drives westward current (i.e., negative *u*) in the surface layer and eastward current in the bottom layer. Although no salinity data are available for days 139–160, the model results show relatively strong stratification with the bottom-surface salinity difference ranging from 5 to 12 psu during this period of large freshwater discharge.

3.3. Salinity

The model reproduces variations in observed salinity well, except that the model under-predicts the surface salinity on days 221–227 and the bottom salinity on days 225–238 (Fig. 5). The under-prediction may be attributable to the open boundary condition for salinity. High salinities up to 36 psu have been observed in the undredged (i.e., outside of ship channel) bottom of lower Mobile Bay (Schroeder and Lysinger, 1979). The present model application employs, because of the lack of data, a temporally constant open boundary condition for salinity with maximum of 35.7 psu (Table 1), which will not allow the model to reproduce intrusions of high salinity Gulf water. On days 225–238, the data show high bottom salinity with virtually no tidal variation and surface salinity with distinct tidal variation, indicative of intrusion of high salinity Gulf water along the bottom (Fig. 5c). After day 238, the model reproduces the observed salinity well for both the total and subtidal components. Both data and model show a larger tidal fluctuation in surface salinity compared to that in bottom salinity, and tropic–equatorial modulation in tidal fluctuation of salinity. Excluding the period of 225–238 d, *ME* (1 psu) and *MAE* (2 psu) are small, and the model skills are 0.80–0.82 and 0.68–0.77 for the total and subtidal components, respectively (Table 3).

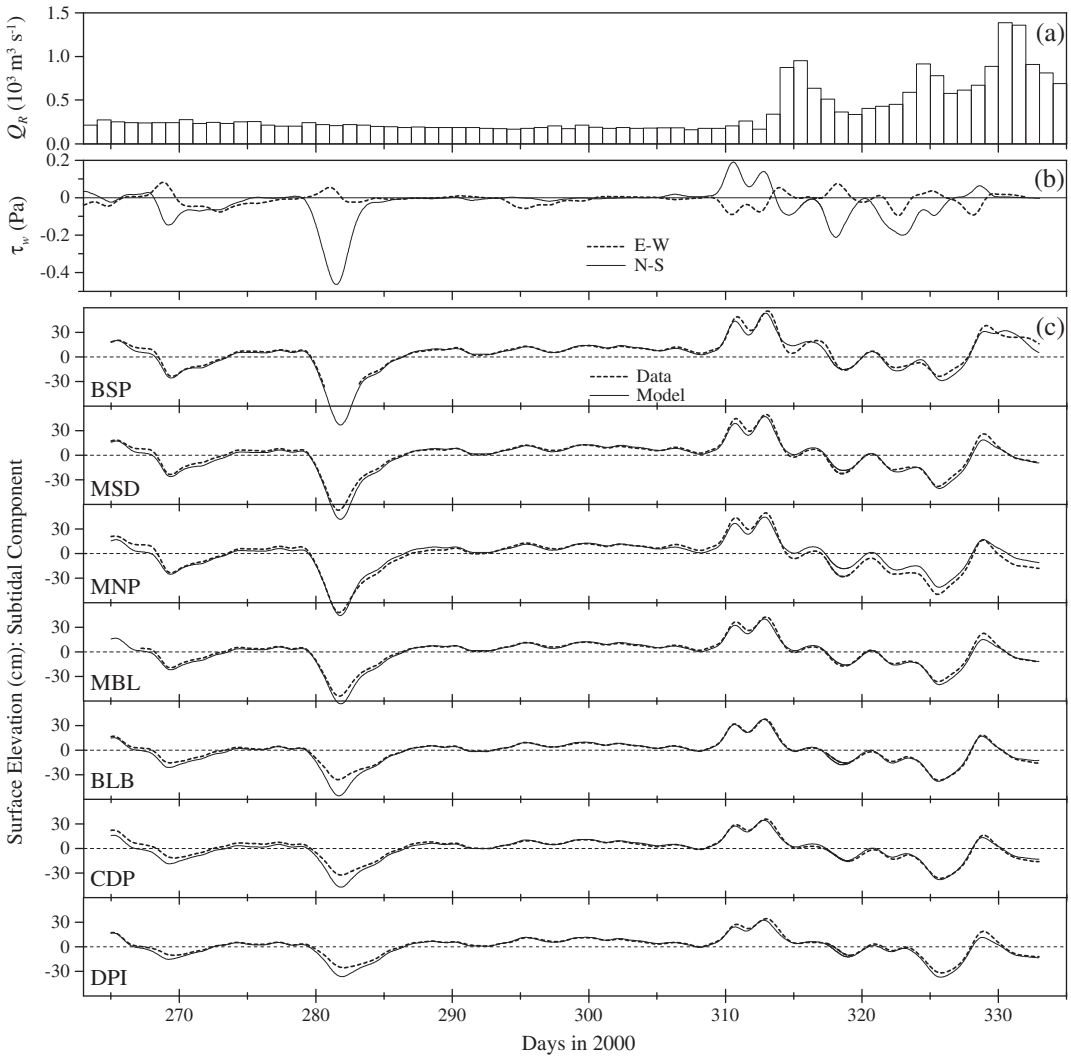

Fig. 3. Daily river discharge (a), low-pass filtered wind stress (b), and model-data comparison for subtidal component of surface elevation at seven tide stations (c).

The model reproduces the bottom-surface salinity difference well for both the total and subtidal components (Fig. 5c, d) with a *ME* of −1 psu, *MAE* of 1–2 psu and the model skills of 0.81–0.82 (Table 3). The high predictive skill in simulating stratification is particularly encouraging since water column stratification turns out to be an important factor influencing salt exchange through MP (Section 4.2). Both data and model show strong stratification with maximum salinity difference of about 15 psu, as has been frequently observed in Mobile Bay (Noble et al., 1996; Park et al., 2007; Schroeder, 1978; Schroeder and Lysinger, 1979). With little variation in river discharge during the period of salinity simulation, stratification is affected by wind conditions. Relatively strong wind weakens stratification, sometimes resulting in a homogeneous water column (e.g., days 262, 269, and 278 in Fig. 5c). On the subtidal time scale, both data and model show relatively weak stratification <5 psu occurring on days 242–250 and 268–280, and strong stratification >5 psu on days 252–266 (Fig. 5d). Vertical mixing may redistribute dissolved and passive particulate materials and thus change their net horizontal transport and distribution (Pringle and Franks, 2001; Shen et al., 1999). Variations in vertical mixing may modify baroclinic circulation, and thus mass transport, in an estuary (Park and Kuo, 1996). A good reproduction of stratification and vertical mixing in lower Mobile Bay, therefore, is encouraging in light of our goal of simulating water and salt exchange through MP and PaH.

4. Estuary–shelf exchange

We analyze the 1991 simulation results to study the characteristics of water and salt exchange through MP and PaH. Note that the mean cross-sectional area of MP (2.9×10^4 m^2) is about five times that of PaH (5.8×10^3 m^2) (Fig. 6). The subtidal volume discharge rate Q_f and salt transport rate F_S through a cross-section A are estimated for MP and PaH using:

$$Q_f = \left\langle \iint u \cdot dA \right\rangle \tag{2}$$

$$F_S = \left\langle \iint uS \cdot dA \right\rangle \tag{3}$$

where u is the normal velocity component, S is salinity, and the angled bracket indicates a 48-h low-pass filter. To gain insight into the controlling mechanisms of salt transport, F_S is decomposed into three components, following Lerczak et al. (2006):

$$\begin{aligned} F_S &= \left\langle \iint (u_0 + u_E + u_T)(S_0 + S_E + S_T) \cdot dA \right\rangle \\ &\approx \left\langle \iint (u_0 S_0 + u_E S_E + u_T S_T) \cdot dA \right\rangle = Q_f S_0 + F_E + F_T \end{aligned} \tag{4}$$

where u and S are decomposed into tidally and cross-sectionally averaged (u_0 and S_0), tidally averaged and cross-sectionally varying

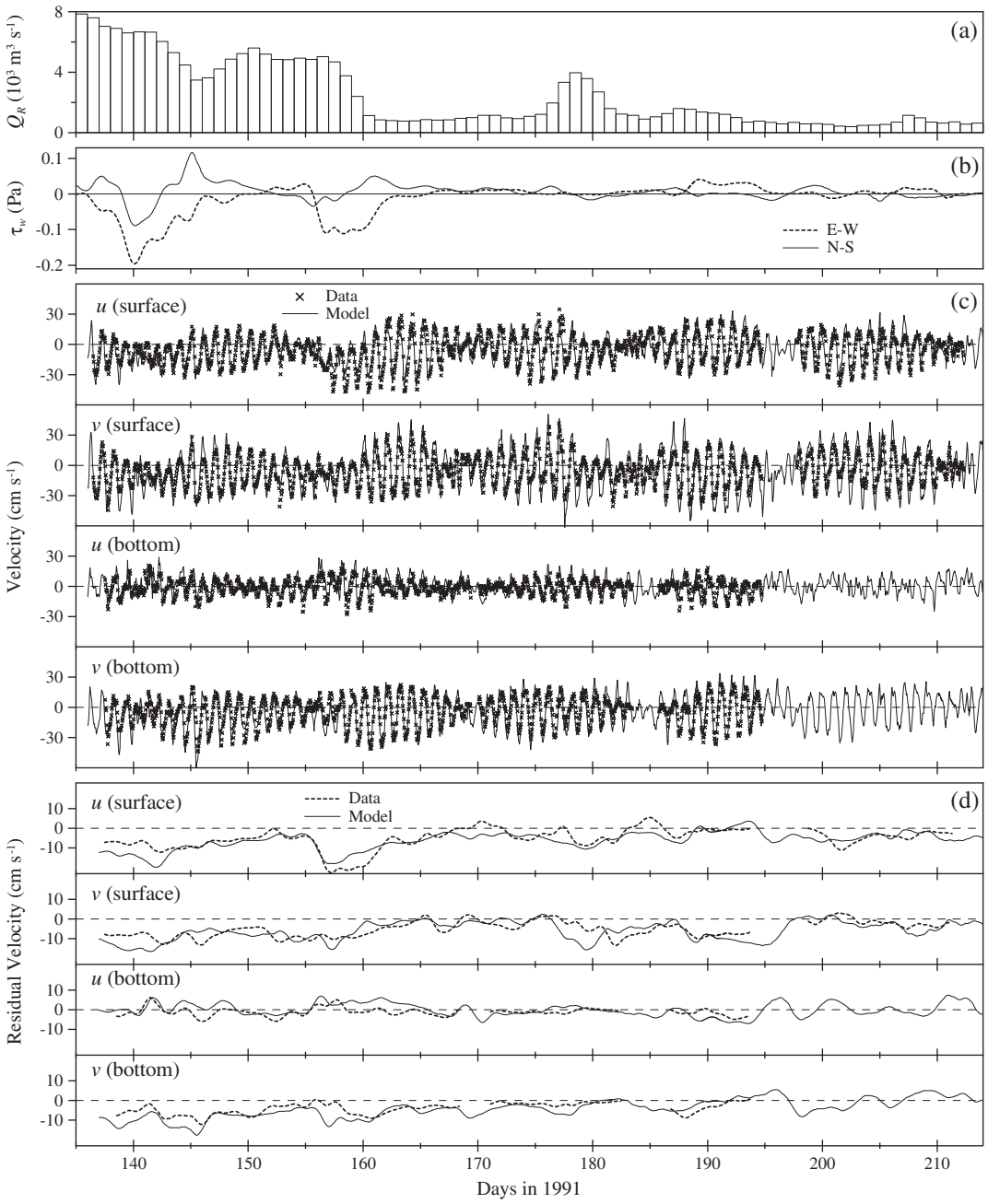

Fig. 4. Daily river discharge (a), low-pass filtered wind stress (b), and model-data comparison for current velocity (c) and for residual velocity (d) at station MB-B. Positive (negative) wind stress in (b) is for south (north) or west (east) wind, and positive (negative) velocity in (c) and (d) is to the north (south) or east (west).

(u_E and S_E), and tidally and cross-sectionally varying (u_T and S_T) components. The three terms in the right-hand side of Eq. 4 represent the subtidal salt fluxes due to cross-sectional average advective transport ($Q_f S_0$), shear dispersion due to vertical and lateral shear transport (F_E), and tidal oscillatory salt transport due to temporal correlations between u and S (F_T).

4.1. Variability in Q_f and F_S

The 1991 simulation period shows a wide range of environmental conditions for river discharge (Fig. 7a) and wind (Fig. 7b). Average Q_f over the simulation period is -1.2×10^3 and -6.7×10^2 m^3 s^{-1} for MP and PaH, respectively (negative discharge indicating outflux from Mobile Bay, i.e., southward through MP and westward through PaH), indicating that MP accounts for 64% of the total net discharge and PaH the remaining 36% on average. Previous studies suggested that the majority (67–85%) of the water exchange occurs through MP (Austin, 1954; Schroeder, 1978). Average F_S over the simulation period is 7.1×10^3 and -7.1×10^3 kg s^{-1} for MP and PaH, respectively; that is, the Bay gains salt through MP and loses about the same amount of salt through PaH on average. Both Q_f and F_S show large temporal variability, with Q_f ranging from -7.3×10^3 to 3.5×10^3 m^3 s^{-1} through MP and -3.7×10^3 to 6.5×10^2 m^3 s^{-1} through PaH (Fig. 7c), and F_S ranging from -1.8×10^5 to 1.3×10^5 kg s^{-1} through MP and -7.2×10^4 to 1.8×10^4 kg s^{-1} through PaH (Fig. 7d). With the range of variation 1–2 orders of magnitude larger than the corresponding mean, the mean values are not so representative of the water and salt exchange through two passes. The dynamics of such large variability are addressed in Sections 4.2 and 4.3.

The power spectra of Q_f and F_S show no peak associated with the tropic–equatorial period, but the instantaneous volume discharge and salt transport rates, which are much larger than the subtidal

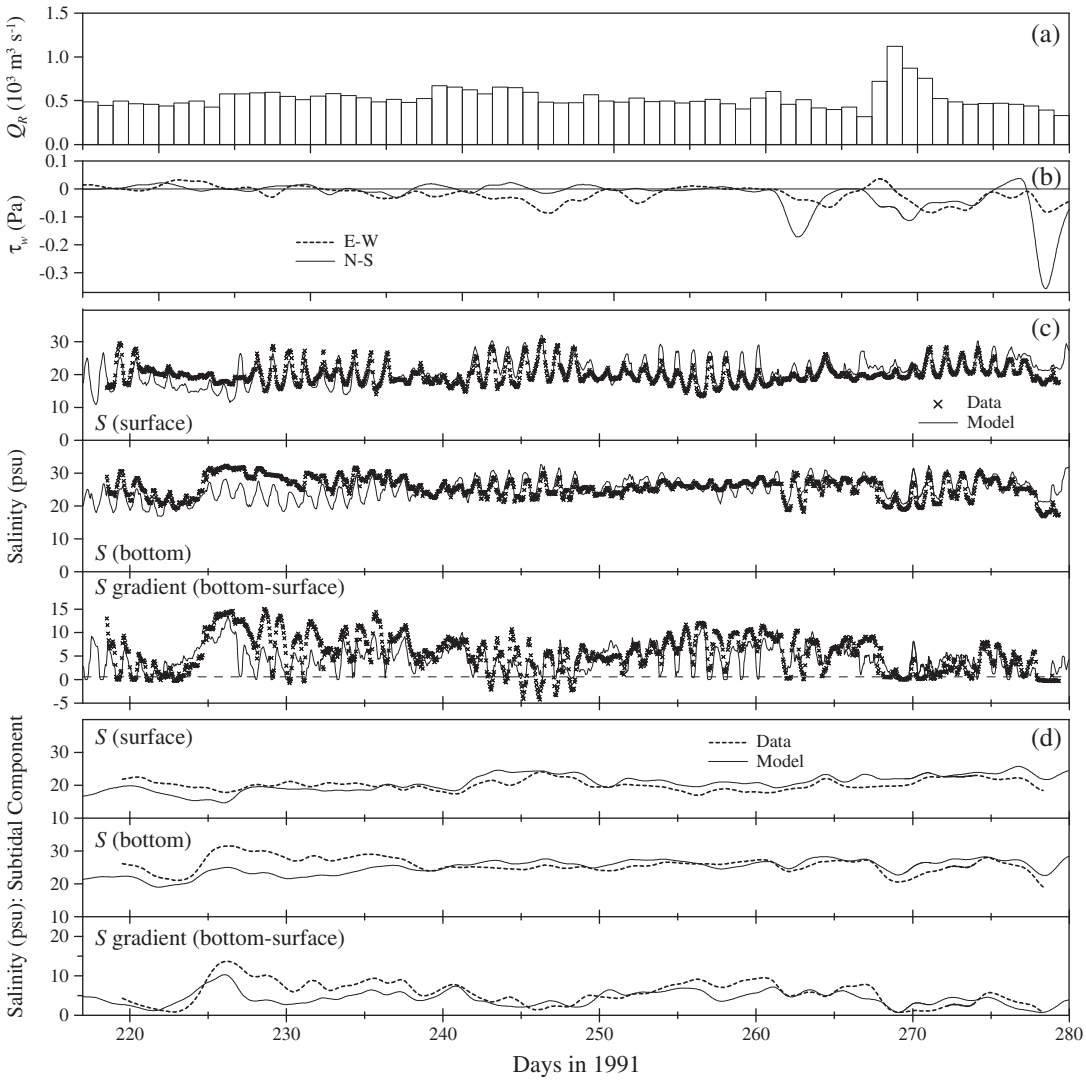

Fig. 5. Daily river discharge (a), low-pass filtered wind stress (b), and model-data comparison for salinity and salinity gradient (c) and for their subtidal components (d) at station MB-B. Positive (negative) wind stress in (b) is for south (north) or west (east) wind.

counterparts, show a distinct tropic–equatorial cycle (not shown). The instantaneous discharge rate varies in amplitude from about 5×10^3 m^3 s^{-1} during equatorial tides to about 2×10^4 m^3 s^{-1} during tropic tides at MP, and from about 1×10^3 m^3 s^{-1} during equatorial tides to about 3×10^3 m^3 s^{-1} during tropic tides at PaH, an order of magnitude less than those at MP. The instantaneous salt transport rate varies in amplitude from about 1×10^5 kg s^{-1} during equatorial tides to about 6×10^5 kg s^{-1} during tropic tides at MP, and from about 1×10^4 kg s^{-1} during equatorial tides to about 4×10^4 kg s^{-1} during tropic tides at PaH, again an order of magnitude less than those at MP.

Both Q_f and F_S show large lateral and vertical variability (not shown). Water and salt are generally transported into the Bay through the ship channel of MP and out of the Bay through the surface layer: see Fig. 6a for the cross-section of MP. Most of the time, water and salt are transported out of the Bay through the shallow PaH. The influx in the channel and the outflux over shoals are in agreement with the previous observations in many other systems (Jay and Smith, 1990; Valle-Levinson, 2008; Valle-Levinson et al., 2009; Wong, 1994). Wind and freshwater discharge, however, can modify these patterns: see Sections 4.2 and 4.3.

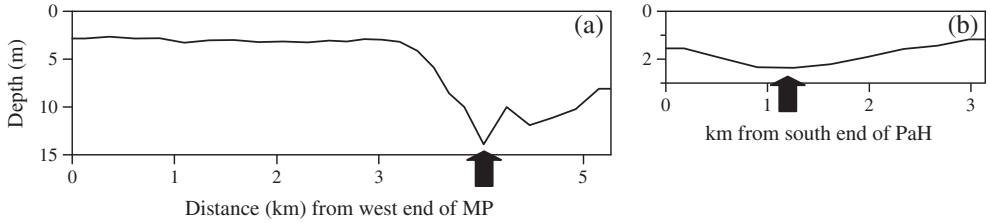

Fig. 6. Cross-sections of Main Pass, MP (a) and Pass-aux-Herons, PaH (b): note that the y-axis (depth) scales are different between (a) and (b). The arrow in (a) indicates the cell location for Figs. 8 and 9, and the arrow in (b) for Fig. 10.

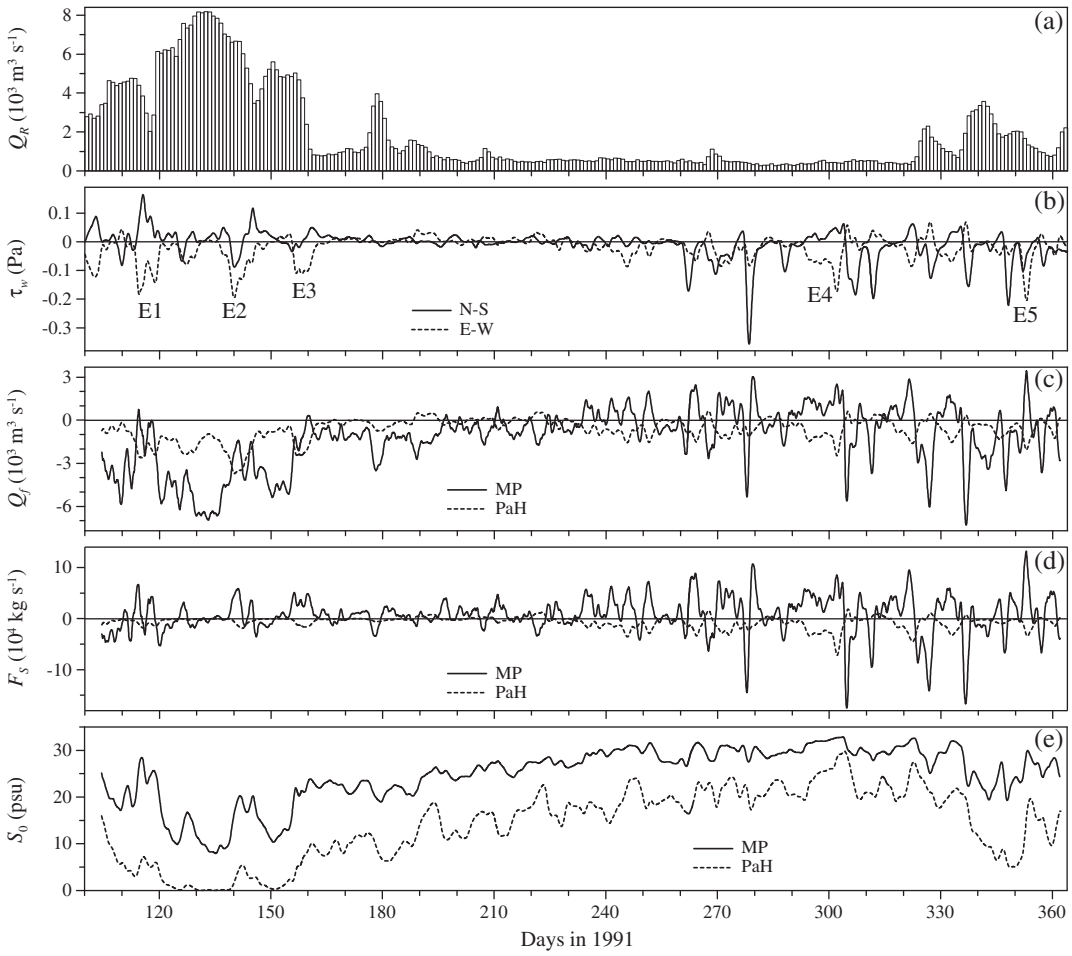

Fig. 7. River discharge (a), wind stress (b), and volume discharge rate Q_f (c), salt transport rate F_S (d), and cross-sectional average salinity S_0 (e) at MP and PaH. Positive (negative) wind stress in (a) is for south (north) or west (east) wind, and positive (negative) flux in (c) and (d) is into (out of) the Bay. E1–E5 in (b) indicate events dominated by east wind.

4.2. Exchange through MP

The volume discharge rate Q_f in Eq. 2 is decomposed into the Eulerian residual and Stokes drift volume discharge rates (Park et al., 2002; Sylaios and Boxall, 1998). Q_f is almost entirely determined by the Eulerian residual discharge rate (Q_E) at MP: $Q_f = 0.99 \cdot Q_E + 74$ ($r^2 = 0.9993$). However, the relative contribution of the three components in Eq. 4 to F_S varies as function of water column stratification. When stratification is relatively weak (days 235–337 in Fig. 8c), F_S is almost entirely determined by the advective salt transport $Q_f S_0$ (Fig. 8a). When stratification is relatively strong (days 104–235 and 337–362), the shear dispersive salt transport F_E and the tidal oscillatory salt transport F_T are at least as important as $Q_f S_0$.

The estuarine salinity S_E at the deep ship channel of MP (Fig. 8c) varies greatly with large variation in stratification. Strong stratification exists on days 104–160 with the bottom-surface salinity difference (ΔS_E) as large as 30 psu, whereas relatively weak stratification exists on days 235–337 with ΔS_E ranging from 0 to 9 psu. Moderate stratification exists on days 160–235 and 337–362 with the respective mean ΔS_E of 13 and 11 psu. Variation in stratification is largely determined by river discharge (Fig. 7a) and shows no relationship with the tropic–equatorial cycle (Fig. 8d). The estuarine flow u_E at the deep ship channel of MP (Fig. 8b) is highly sheared, as has been observed in Mobile Bay (Noble et al., 1996; Park et al., 2007) and shows large variability. Landward u_E persists in the lower layer and its maximum occurring at mid-depth, consistent with the observation in Lerczak et al. (2006), exceeds 0.5 m s^{-1}. At the surface, u_E is seaward most of the time resulting in two-layer circulation, but wind can shift its direction, particularly when the water column is weakly stratified. The level of stratification also affects the pattern of variation in u_E, as we will show in the remainder of this section.

4.2.1. Strong stratification

Large river discharge on days 104–160 with peak values >8000 m^3 s^{-1} (Fig. 7a) results in strong stratification with ΔS_E ranging from 15 to 30 psu (Fig. 8c); days 115–120 are exceptions when a strong southeast wind (Fig. 7b) pushes surface water landward (Fig. 8b) and enhances vertical mixing to reduce stratification (Fig. 8c). Large river discharge also increases seaward Q_f (Fig. 7c), which, despite a reduced cross-sectional average salinity S_0 (Fig. 7e), results in the seaward $Q_f S_0$ at MP to range from -2.7×10^4 to -8.3×10^4 kg s^{-1} with a mean of -5.5×10^4 kg s^{-1} on days 122–156 (Fig. 8a).

During this period of strong stratification, u_E shows a distinct tropic–equatorial cycle. The exchange flow Δu_E, defined as the difference between the surface and bottom u_E, varies by an order of magnitude from 0.07 m s^{-1} during tropic tides to 0.77 m s^{-1} during equatorial tides (Fig. 8b). While S_E shows no relationship with the tropic–equatorial cycle, this large variation in u_E contributes to an order of magnitude variation in F_E (Fig. 8a). During equatorial tides, the landward F_E, peaking at 8.7×10^4 kg s^{-1}, overcomes $Q_f S_0$ to result in the net landward F_S. During tropic tides, F_E is much smaller than $Q_f S_0$. Lerczak et al. (2006) also observed the landward F_E exceeding the seaward $Q_f S_0$ during neap tides, but the order of magnitude fluctuations in S_E, rather than the smaller variations in u_E, over the spring–neap cycle was the principal cause of the spring–neap variations in F_E in the Hudson River estuary. In Mobile Bay, during the

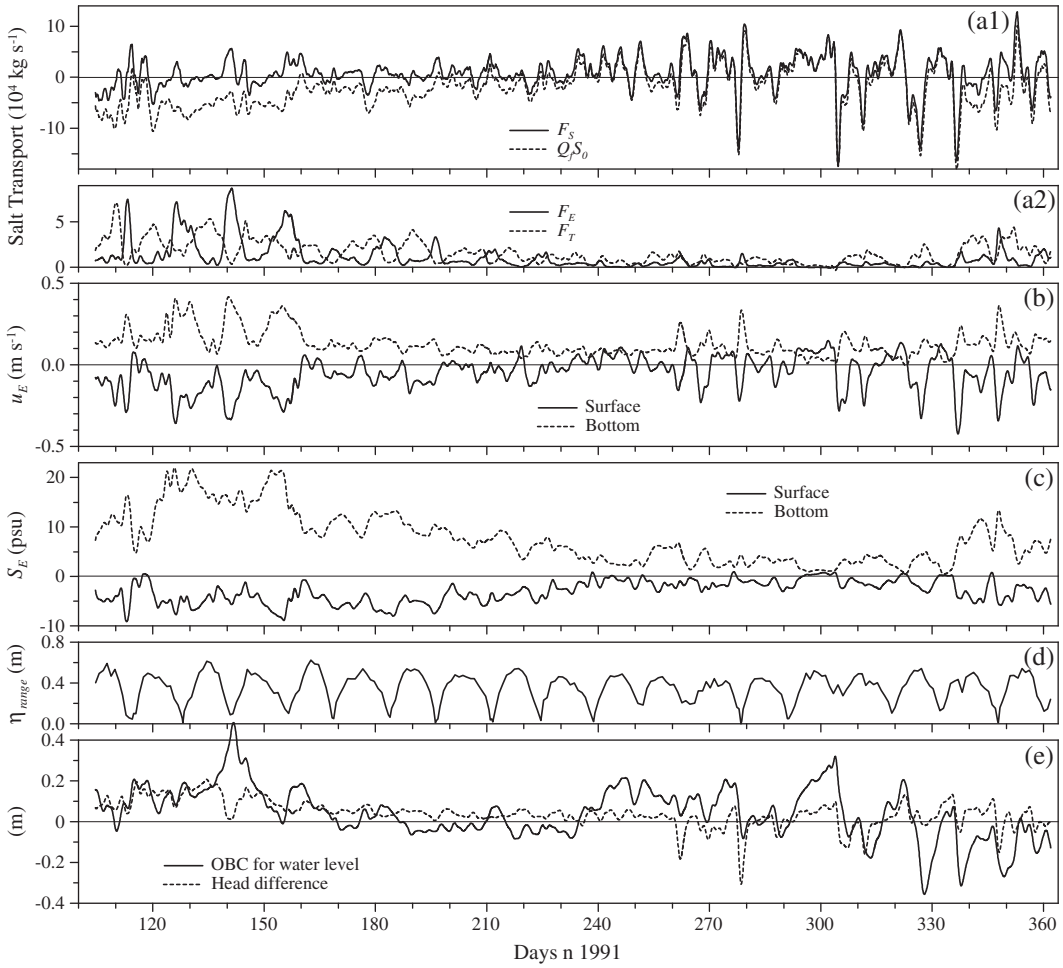

Fig. 8. Salt transport rate F_S and its three components Q_f, S_0, F_E and F_T through MP (a), subtidal estuarine exchange flow u_E (b) and salinity S_E (c), tidal range after the subtidal component being removed (d), and open boundary condition for water level and head difference (e): (b)–(d) are at the deep ship channel of MP (see Fig. 6a for location), and head difference in (e) is the difference in the modeled surface elevation between the Mobile River entrance (see Fig. 1) and MP, with positive values indicating higher surface at the Mobile River entrance. Positive (negative) flux in (a) and positive (negative) velocity in (b) are into (out of) the Bay. Note that the y-axis scales are different between (a1) and (a2), and that the solid line in (a1) is identical to the solid line in Fig. 7d.

times of large river discharge, strong stratification results in a highly sheared two-layer system, as argued by Ryan et al. (1997). During equatorial tides with virtually no tidal currents, there is minimal interaction between the upper and lower layers, which is likely responsible for enhanced seaward flow of fresher surface water and landward return flow of saltier bottom water (Fig. 8b), thus generating strong Δu_E and peaks in F_E.

During the period of strong stratification, the landward F_T shows a distinct tropic–equatorial cycle. During tropic tides, the landward F_T, peaking at 7.1×10^4 kg s^{-1}, is as large as the seaward Q_fS_0, thus resulting in F_S fluctuating around zero (Fig. 8a). This is consistent with the observations in the lower Columbia River estuary (Jay and Smith, 1990: Fig. 20) in that F_T, being larger than the sum of Q_fS_0 and F_E, resulted in the net landward F_S, and that F_T increased with river discharge as the flow became more stratified. Lerczak et al. (2006: Fig. 8) in the Hudson River estuary found that the magnitude of F_T varied over the spring–neap cycle, in agreement with our finding, but the observed F_T was smaller than either Q_fS_0 or F_E. In Mobile Bay, during the times of large river discharge, the tidal salinity S_T at the ship channel of MP shows great tidal fluctuation with its amplitude varying by 25–30 psu during tropic tides; for comparison, it is <10 psu during the times of sustained low river discharge. Such large intratidal variation in S_T, combined with the phase difference between S_T and u_T less than quadrature, results in large landward F_T, comparable to Q_fS_0, during tropic tides.

4.2.2. Moderate stratification

With seasonal decreases in river discharge beyond day 160 (Fig. 7a), stratification continues to weaken but still remains with a mean ΔS_E of 13 psu on days 160–235 (Fig. 8c). During this period of moderate stratification, both F_E and F_T get weaker but are still comparable to Q_fS_0, which also reduces with decreasing river discharge. As in the period of strong stratification, F_E peaks at 3.3×10^4 kg s^{-1} during equatorial tides and F_T peaks at 4.1×10^4 kg s^{-1} during tropic tides, respectively, balancing the seaward Q_fS_0 and thus resulting in a very small F_S (Fig. 8a). On days 337–362, a similar level of stratification (mean ΔS_E of 11 psu) exists with seasonal increases in river discharge. F_E and F_T are of a similar magnitude and still are out of phase in the tropic–equatorial cycle, but are too small to balance Q_fS_0, which shows large peaks caused by wind events; see Section 4.2.3 for the effect of wind.

4.2.3. Relatively weak stratification

River discharge is seasonally low on days 200–322 with a mean of 500 m^3 s^{-1} (Fig. 7a), resulting in relatively weak stratification with ΔS_E ranging from 0 to 9 psu on days 235–337 (Fig. 8c). During this period of relatively weak stratification, F_S at MP is almost entirely determined by Q_fS_0 with little contribution from F_E or F_T (Fig. 8a): $F_S = 0.95\cdot Q_fS_0 + 1.0\times10^4$ ($r^2 = 0.98$). With little variation in S_0 during this period (Fig. 7e), Q_fS_0 is well correlated with Q_f (Fig. 7c) with an r-value of 0.997. The peaks in Q_f, and thus Q_fS_0 and F_S, are sharper than

those during the period of strong stratification, and their variability is mostly associated with wind events (Fig. 7b).

During the period of relatively weak stratification on days 235–337, $Q_f S_0$ shows a maximum correlation ($r = 0.69$) with the north–south wind at a time lag of 18 h. To see the details, we focus on the conditions during days 255–310 that have five relatively strong north wind events with peak north wind stresses ranging from 0.1 to 0.36 Pa (N1–N5 in Fig. 9a). The north wind pushes water southward, increasing outflux $Q_f S_0$ through MP (Fig. 9b), and raises water level downstream toward MP, producing negative peaks in along-Bay surface slope (Fig. 9f). Toward the end of the wind events, the barotropic pressure gradient overcomes the wind-driven outflux, generating a return flux into Mobile Bay. This barotropic (water level) adjustment results in the sharp peaks in $Q_f S_0$, which is consistent with Chen and Sanford (2009: Fig. 7). This also supports the suggestion in Schroeder and Wiseman (1986) that the shallow and closed geometry of Mobile Bay may allow north wind stress to generate an along-Bay surface slope, which produces a barotropic pressure gradient and drives the mean flow.

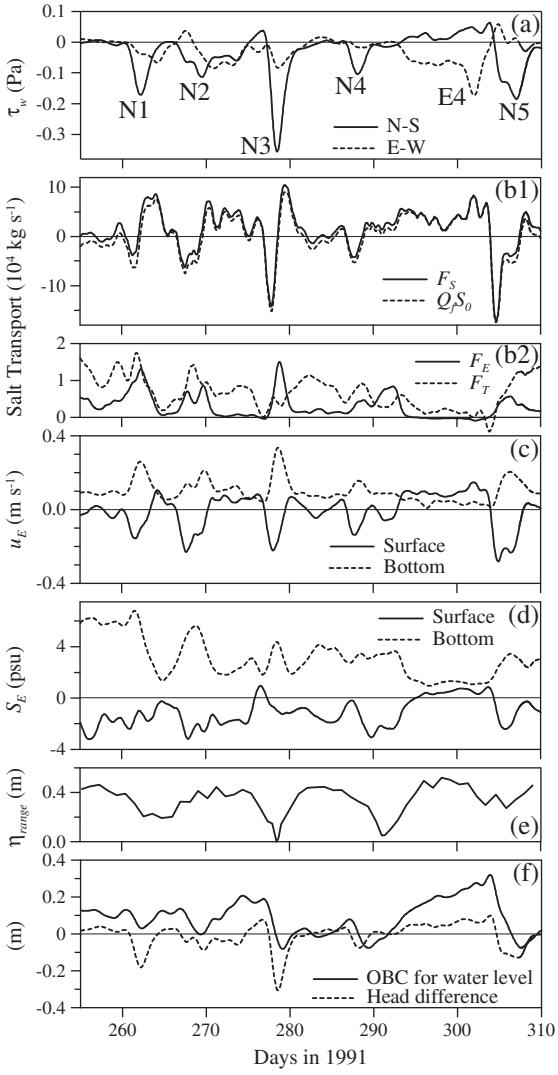

Fig. 9. Conditions on days 255–310 for the wind stress (a), salt transport rate F_S and its three components $Q_f S_0$, F_E and F_T through MP (b), subtidal estuarine exchange flow u_E (c) and salinity S_E (d), tidal range after removal of the subtidal component (e), and open boundary condition for water level and head difference (f): (c)–(e) are at the deep ship channel of MP (see Fig. 6a for location), and head difference in (f) is the difference in the modeled surface elevation between the Mobile River entrance (see Fig. 1) and MP, with positive values indicating higher surface at the Mobile River entrance. Positive (negative) wind in (a) is for south (north) wind. Positive (negative) flux in (b) and positive (negative) velocity in (c) are into (out of) the Bay. Note that the y-axis scales are different from their counterparts in Figs. 7 and 8. N1–N5 and E4 in (a) indicate events dominated by north wind and east wind, respectively.

Both observations in the York River estuary (Scully et al., 2005) and idealized model results (Chen and Sanford, 2009) showed that moderate down-estuary wind enhances subtidal vertical velocity shear and increases stratification if wind straining outcompetes direct wind mixing. In Mobile Bay, the north (down-estuary) wind events do enhance Δu_E, increasing the vertical velocity shear from zero to $>0.5\ \mathrm{m\ s^{-1}}$ during the event N3 (Fig. 9c). The north wind events also increase the stratification, with the exception of N4 that shows decreasing ΔS_E (Fig. 9d). Consequently, the north wind events are associated with peaks in F_E, but even the largest peak, $1.5\times 10^4\ \mathrm{kg\ s^{-1}}$ during the event N3, is an order of magnitude smaller than $Q_f S_0$ (Fig. 9b). A south wind occurs mostly with an east wind, with the latter stronger than the former (Fig. 7b), and thus the response to an east wind (see below) makes it difficult to examine the effect of the south (up-estuary) wind. It is interesting to note that F_T is as large as F_E (Fig. 9b), and is in phase with tropic tides (Fig. 9e). One exception is a tropic tide centered on day 299 when F_T is virtually zero, even with some negative (seaward) values, which is attributable to an east wind event as shown below.

All east wind events are associated with increases in coastal water level (positive peaks in the water level open boundary condition in Fig. 8e). To see the details, we focus on the conditions on days 295–303 that have a relatively strong east wind event (E4 in Fig. 9a). This wind event, persisting over 8 d with east wind stress values >0.07 Pa and a peak stress >0.17 Pa, induces onshore Ekman transport and thus results in coastal set-up (a broad positive peak in Fig. 9f). Onshore transport of saline Gulf water, then, causes landward u_E throughout the water column (Fig. 9c) and results in a relatively well-mixed water column where the salinities at both the surface and the bottom layers are higher than the cross-sectional average salinity S_0 (Fig. 9d). During this period of relatively strong east wind, F_S at MP is almost entirely determined by $Q_f S_0$ with a negligible contribution from F_E or F_T (Fig. 9b). Other east wind events E1, E3 and E5 (Fig. 7b) show the same pattern of coastal set-up (Fig. 8e), landward u_E throughout the water column (Fig. 8b) and reduced stratification (Fig. 8c); the direct response to the south wind component also contributes to landward u_E at the surface for E1. Another east wind event E2, however, does not follow the same pattern. Despite having a peak east wind stress of 0.2 Pa and the water level at the open boundary being the highest, the strong stratification with $\Delta S_E > 21$ psu (Fig. 8d) prevents a uniform response in the water column and results in a distinct two-layer flow structure with large Δu_E (Fig. 8c). No strong west wind events occur during the simulation period. Coastal sea level set-up or set-down by alongshore wind-induced onshore or offshore Ekman transport has been observed to influence the subtidal exchange in the northern Gulf of Mexico estuaries (Chuang and Wiseman, 1983; Schroeder and Wiseman, 1986; Smith, 1977) and other estuarine systems (e.g., Ryan and Noble, 2007; Wong and Moses-Hall, 1998; Wong and Valle-Levinson, 2002).

4.3. Exchange through PaH

Water (Fig. 10b) and salt (Fig. 10c) are primarily transported out of the Bay throughout the shallow PaH (mean depth <2.4 m in Fig. 6b). As in MP, Q_f is almost entirely determined by the Eulerian volume discharge rate at PaH: $Q_f = 1.0 \cdot Q_E + 25$ ($r^2 = 0.999$). Q_f (Fig. 10b) is well correlated with east–west wind (Fig. 10a) with $r = 0.86$. The correlation becomes stronger during the dry period with relatively low river discharge: e.g., $r = 0.93$ on days 190–324.

Unlike MP, F_S at PaH is almost identical to $Q_f S_0$ throughout the simulation period with a negligible contribution from F_E or F_T: $F_S = 1.0 \cdot Q_f S_0 + 91$ ($r^2 = 0.998$). Large river discharge increases the outflux Q_f (Fig. 10b) but also decreases S_0 considerably (Fig. 7e):

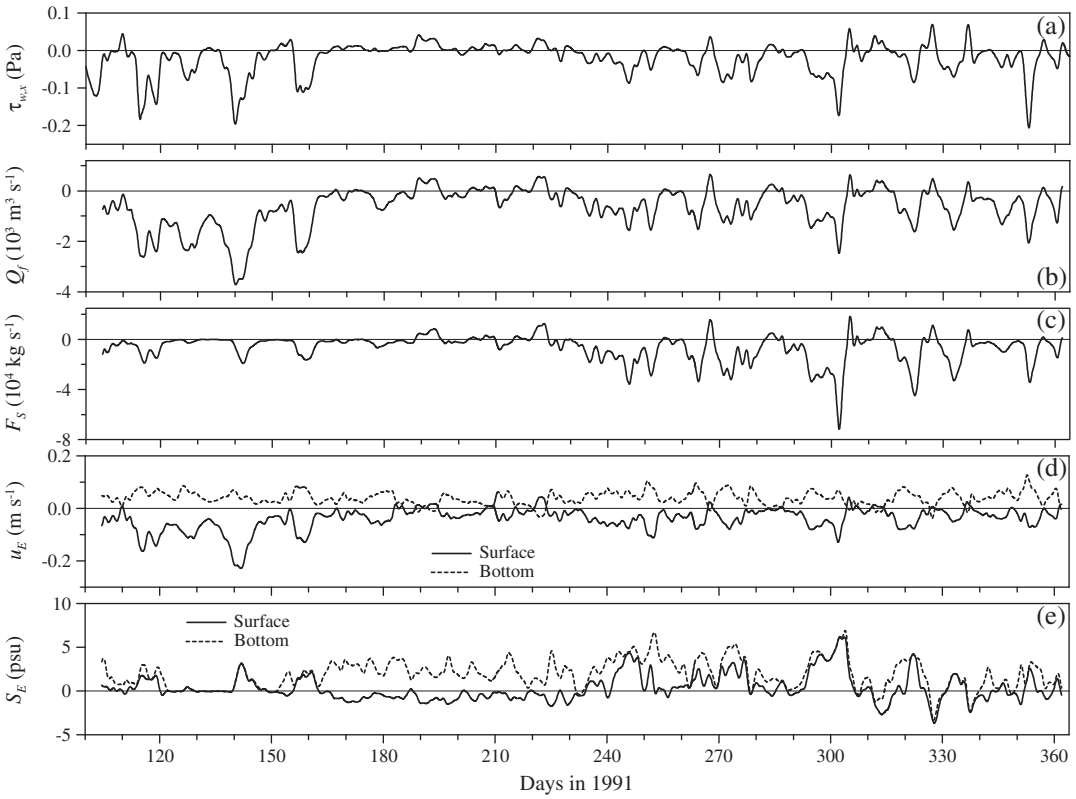

Fig. 10. East–west wind stress (a), volume discharge Q_f (b) and salt transport F_S (c) rates through PaH, and subtidal estuarine exchange flow u_E (d) and salinity S_E (e) at the channel of MP (see Fig. 6b for location). Positive (negative) wind in (a) is for west (east) wind. Positive (negative) flux in (b) and (c), and positive (negative) velocity in (d) are into (out of) the Bay. Note that (b) and (c) are identical to the dashed lines in Fig. 7c and d, respectively.

note that the water column becomes virtually fresh on days 120–140 (Fig. 10e) when river discharge is $>6000\ m^3\ s^{-1}$. Despite this large increase in Q_f, a drastic decrease in S_0 results in relatively small Q_fS_0 with its peak magnitude $<1.9\times10^4\ kg\ s^{-1}$ on days 104–183 (Fig. 10c). During the dry period, S_0 does not vary much and Q_fS_0 is well correlated with Q_f, with $r=0.98$ on days 190–324.

The estuarine flow u_E at PaH (Fig. 10d) shows a two-layer circulation most of the time, but its strength is much weaker ($\Delta u_E<0.04\ m\ s^{-1}$) when compared to that at MP. The estuarine salinity S_E (Fig. 10e) shows much weaker stratification (mean ΔS_E of 2 psu). Both u_E and S_E do respond to the east–west wind, although F_E is almost zero because variations in u_E and S_E are very small. The east wind events (e.g., around days 140 and 301) bring the lower Bay water to PaH, thus enhancing westward surface u_E and strengthening Δu_E. Since the lower Bay water is associated with higher salinity from the Gulf, S_E increases throughout the water column owing to the shallow depth and strong wind. The west wind events (e.g., around days 267 and 306) pushes surface water eastward, reducing Δu_E and S_E, and the shallow water column is again well mixed. Because of minimal intratidal variations in S_T (usually <5 psu), F_T is virtually zero at PaH.

5. Conclusions

A three-dimensional hydrodynamic model is applied to the tidal Mobile Bay system to investigate the characteristics of the subtidal exchange of water and salt through MP between Mobile Bay and the northern Gulf of Mexico and through PaH between Mobile Bay and eastern Mississippi Sound. The following conclusions are drawn from this study.

1) On average, more water leaves the Bay through MP than through PaH and the Bay gains salt through MP and loses about the same amount of salt through PaH. However, both the volume discharge rate Q_f and the salt transport rate F_S vary greatly in response to wind and river discharge with the range of variation 1–2 orders of magnitude larger than the corresponding mean.
2) Stratification, which shows great variability largely in response to river discharge, plays a key role at MP. Large river discharge increases seaward Q_f but decreases the cross-sectional average salinity S_0, resulting in moderate increases in the seaward advective salt transport Q_fS_0. During the period of strong stratification, a highly sheared two-layer system generates a highly variable exchange flow with Δu_E varying by an order of magnitude during the tropic–equatorial cycle. During equatorial tides, then, the landward shear dispersive salt transport F_E peaks, overcoming Q_fS_0 and thus resulting in a net landward F_S. During the period of strong stratification, the tidal salinity S_T at the ship channel shows large tidal fluctuation with its amplitude varying by 25–30 psu during tropic tides. This allows the landward tidal oscillatory salt transport F_T to peak during tropic tides, which balances Q_fS_0 and thus results in near-zero F_S.
3) During the period of relatively weak stratification, F_S at MP is almost entirely determined by Q_fS_0 with little contribution from F_E or F_T, and Q_fS_0 is well correlated with Q_f as S_0 varies little during this period. The variability in Q_fS_0 is well correlated with north–south wind, which is associated with the barotropic (water level) adjustment. The down-estuary (north) wind events increase Δu_E and ΔS_E, resulting in peaks in F_E, in agreement with previous studies, but the peaks are an order of magnitude smaller than Q_fS_0 at MP. East (along-shelf) wind events induce onshore Ekman transport and thus coastal sea level set-up, resulting in landward flow throughout the relatively well-mixed water column and thus making F_S almost entirely determined by Q_fS_0 with a negligible contribution from F_E or F_T.
4) Stratification is weak at the shallow PaH with a mean ΔS_E of 2 psu. Then, F_S at PaH is almost identical to Q_fS_0 throughout the simulation period with a negligible contribution from F_E or F_T. Q_f is well

correlated with east–west wind, with the correlation becoming stronger during the dry period with relatively low river discharge.

Acknowledgments

We thank the Mobile District of the U.S. Army Corps of Engineers for sharing the bathymetry and surface elevation data. We thank H.-S. Jung and B. Dzwonkowski for their help in setting-up the model and post-processing the model results, and W.W. Schroeder for providing helpful discussions on earlier versions of the manuscript. This study was funded by the National Marine Fisheries Service, NOAA (via a grant from University of South Alabama's Alabama Oyster Reef Restoration Program) and the NSF Northern Gulf Coastal Hazards Collaboratory (award number EPS-1010607).

References

Austin Jr., G.B., 1954. On the circulation and tidal flushing of Mobile Bay, Alabama, part 1. Technical Report 12. Texas A&M Research Foundation, College Station, TX.
Boon, J.D., 2004. Secrets of the Tide: Tide and Tidal Current Analysis and Applications, Storm Surges and Sea Level Trends. Horwood Publishing, Chichester, UK.
Chen, S.-N., Sanford, L.P., 2009. Axial wind effects on stratification and longitudinal salt transport in an idealized partially mixed estuary. J. Phys. Oceanogr. 39, 1905–1920.
Chuang, W.-S., Wiseman Jr., W.J., 1983. Coastal sea level response to frontal passages on the Louisiana–Texas shelf. J. Geophys. Res. 88, 2615–2620.
Galperin, B., Kantha, L.H., Hassid, S., Rosati, A., 1988. A quasi-equilibrium turbulent energy model for geophysical flows. J. Atmos. Sci. 45, 55–62.
Goodrich, D.M., 1988. On meteorologically induced flushing in three U.S. east coast estuaries. Estuar. Coast. Shelf Sci. 26, 111–121.
Hamrick, J.M., 1992. A three-dimensional environmental fluid dynamics computer code: theoretical and computational aspects. Special Report 317. Virginia Institute of Marine Science, Gloucester Point, VA.
Hamrick, J.M., 1996. User's manual for the environmental fluid dynamics computer code. Special Report 331. Virginia Institute of Marine Science, Gloucester Point, VA.
Hare, J.A., Thorrold, S., Walsh, H., Reiss, C., Valle-Levinson, A., Jones, C., 2005. Biophysical mechanisms of larval fish ingress into Chesapeake Bay. Mar. Ecol. Prog. Ser. 303, 295–310.
Jay, D.A., Smith, J.D., 1990. Circulation, density distribution and neap-spring transitions in the Columbia River Estuary. Prog. Oceanogr. 25, 81–112.
Ji, Z.-G., Morton, M.R., Hamrick, J.M., 2001. Wetting and drying simulation of estuarine processes. Estuar. Coast. Shelf Sci. 53, 683–700.
Lerczak, J., Geyer, W.R., Chant, R.J., 2006. Mechanisms driving the time-dependent salt flux in a partially stratified estuary. J. Phys. Oceanogr. 36, 2296–2311.
Lohrenz, S.E., Fahnenstiel, G.L., Redalje, D.G., Lang, G.A., Chen, X., Dagg, M.J., 1997. Variations in primary production of northern Gulf of Mexico continental shelf water linked to nutrient inputs from the Mississippi River. Mar. Ecol. Prog. Ser. 155, 45–54.
Lowery, T.A., 1988. Difference equation-based estuarine flushing model application to U.S. Gulf of Mexico estuaries. J. Coast. Res. 14, 185–195.
MacDonald, D.G., 2006. Estimating an estuarine mixing and exchange ratio from boundary data with application to Mt. Hope Bay (Massachusetts/Rhode Island). Estuar. Coast. Shelf Sci. 70, 326–332.
Mellor, G.L., Yamada, T., 1982. Development of a turbulence closure model for geophysical fluid problems. Rev. Geophys. Space Phys. 20, 851–875.
Morgan, S.G., Zimmer-Faust, R.K., Heck Jr., K.L., Coen, L.D., 1996. Population regulation of blue crabs *Callinectes sapidus* in the northern Gulf of Mexico: postlarval supply. Mar. Ecol. Prog. Ser. 133, 73–88.
Mortazavi, B., Iverson, R.L., Huang, W., Lewis, F.G., Caffrey, J.M., 2000. Nitrogen budget of Apalachicola Bay, a bar-built estuary in the northeastern Gulf of Mexico. Mar. Ecol. Prog. Ser. 195, 1–14.
Noble, M.A., Schroeder, W.W., Wiseman Jr., W.J., Ryan, H.F., Gelfenbaum, G., 1996. Subtidal circulation patterns in a shallow, highly stratified estuary: Mobile Bay, Alabama. J. Geophys. Res. 101, 25689–25703.
Park, K., Kuo, A.Y., 1996. Effects of variation in vertical mixing on residual circulation in narrow, weakly nonlinear estuaries. In: Aubrey, D.G., Friedrichs, C.T. (Eds.), Buoyancy Effects on Coastal and Estuarine Dynamics, Coastal and Estuarine Studies 53. AGU, Washington, DC, pp. 301–317.
Park, K., Oh, J.-H., Kim, H.-S., Im, H.-H., 2002. Case study: mass transport mechanism in Kyunggi Bay around Han River mouth, Korea. J. Hydraul. Eng. 128, 257–267.
Park, K., Kim, C.-K., Schroeder, W.W., 2007. Temporal variability in summertime bottom hypoxia in shallow areas of Mobile Bay, Alabama. Estuaries Coasts 30, 54–65.
Pringle, J.M., Franks, P.J.S., 2001. Asymmetric mixing transport: a horizontal transport mechanism for sinking plankton and sediment in tidal flows. Limnol. Oceanogr. 46, 381–391.
Rabalais, N.N., Burditt Jr., F.R., Coen, L.D., Cole, B.E., Eleuterius, C., Heck Jr., K.L., McTigue, T.A., Morgan, S.G., Perry, H.M., Truesdale, F.M., Zimmer-Faust, R.K., Zimmerman, R.J., 1995. Settlement of *Callinectes sapidus* megalopae on artificial collectors in four Gulf of Mexico estuaries. Bull. Mar. Sci. 57, 855–876.
Ryan, H.F., Noble, M.A., 2007. Sea level fluctuations in central California at subtidal to decadal and longer time scales with implications for San Francisco Bay, California. Estuar. Coast. Shelf Sci. 73, 538–550.
Ryan, H.F., Noble, M.A., Williams, E.A., Schroeder, W.W., Pennock, J.R., Gelfenbaum, G., 1997. Tidal current shear in a broad, shallow, river-dominated estuary. Cont. Shelf Res. 17, 665–688.
Schroeder, W.W., 1978. Riverine influence on estuaries: a case study. In: Wiley, M.L. (Ed.), Estuarine Interactions. Academic Press, NY, pp. 347–364.
Schroeder, W.W., Lysinger, W.R., 1979. Hydrography and circulation of Mobile Bay. In: Loyacano, H.A., Smith, J.P. (Eds.), Symposium on the Natural Resources of the Mobile Bay Estuary. Mobile District of the U.S. Army Corps of Engineers, Mobile, AL, pp. 75–94.
Schroeder, W.W., Wiseman Jr., W.J., 1986. Low-frequency shelf-estuarine exchange processes in Mobile Bay and other estuarine systems on the northern Gulf of Mexico. In: Wolfe, D.A. (Ed.), Estuarine Variability. Academic Press, NY, pp. 355–366.
Schroeder, W.W., Wiseman Jr., W.J., 1999. Geology and hydrodynamics of Gulf of Mexico estuaries. In: Bianchi, T.S., Pennock, J.R., Twilley, R.R. (Eds.), Biogeochemistry of Gulf of Mexico Estuaries. John Wiley & Sons, NY, pp. 3–28.
Scully, M.E., Friedrichs, C.T., Brubaker, J.M., 2005. Control of estuarine stratification and mixing by wind-induced straining of the estuarine density field. Estuaries 28, 321–326.
Sheldon, J.E., Alber, M., 2002. A comparison of residence time calculations using simple compartment models of the Altamaha River estuary, Georgia. Estuaries 25, 1304–1317.
Shen, J., Boon, J.D., Kuo, A.Y., 1999. A modeling study of a tidal intrusion front and its impact on larval dispersion in the James River estuary, Virginia. Estuaries 22, 681–692.
Simons, R.D., Monismith, S.G., Johnson, L.E., Winkler, G., Saucier, F.J., 2006. Zooplankton retention in the estuarine transition zone of the St. Lawrence Estuary. Limnol. Oceanogr. 51, 2621–2631.
Smith, N.P., 1977. Meteorological and tidal exchanges between Corpus Christi Bay, Texas, and the northwestern Gulf of Mexico. Estuar. Coast. Mar. Sci. 5, 511–520.
Spitzer, P.M., Heck Jr., K.L., Valentine, J.F., 2003. Then and now: a comparison of patterns in blue crab post-larval abundance and post-settlement mortality during the early and late 1990s in the Mobile Bay system. Bull. Mar. Sci. 72, 435–452.
Stumpf, R.P., Gelfenbaum, G., Pennock, J.R., 1993. Wind and tidal forcing of a buoyant plume, Mobile Bay, Alabama. Cont. Shelf Res. 13, 1281–1301.
Sylaios, G., Boxall, S.R., 1998. Residual currents and flux estimates in a partially-mixed estuary. Estuar. Coast. Shelf Sci. 46, 671–682.
Valle-Levinson, A., 2008. Density-driven exchange flow in terms of the Kelvin and Ekman numbers. J. Geophys. Res. 113, C04001. doi:10.1029/2007JC004144.
Valle-Levinson, A., Lwiza, K.M.M., 1995. The effects of channels and shoals on exchange between the Chesapeake Bay and the adjacent ocean. J. Geophys. Res. 100, 18551–18563.
Valle-Levinson, A., Wong, K.-C., Bosley, K.T., 2001. Observations of the wind-induced exchange at the entrance to Chesapeake Bay. J. Mar. Res. 59, 391–416.
Valle-Levinson, A., Gutierrez de Velasco, G., Trasviña, A., Souza, A.J., Duranzo, R., Mehta, A.J., 2009. Residual exchange flows in subtropical estuaries. Estuaries Coasts 32, 54–67.
Willmott, C.J., 1982. Some comments on the evaluation of model performance. Bull. Am. Meteorol. Soc. 63, 1309–1313.
Wiseman Jr., W.J., Schroeder, W.W., Dinnel, S.P., 1988. Shelf-estuarine water exchanges between the Gulf of Mexico and Mobile Bay, Alabama. Am. Fish. Soc. Symp. 3, 1–8.
Wong, K.-C., 1994. On the nature of transverse variability in a coastal plain estuary. J. Geophys. Res. 99, 14209–14222.
Wong, K.-C., Moses-Hall, J.E., 1998. On the relative importance of the remote and local wind effects to the subtidal variability on a coastal plain estuary. J. Geophys. Res. 103, 18393–18404.
Wong, K.-C., Valle-Levinson, A., 2002. On the relative importance of the remote and local wind effects on the subtidal exchange at the entrance to the Chesapeake Bay. J. Mar. Res. 60, 477–498.